Real, M.; Hedinger, R.; Pla Moreno, B.; Onder, C. (2021). Modelling three-way catalytic converter oriented to engine cold-start conditions. International Journal of Engine Research. 22(2):640-651. https://doi.org/10.1177/1468087419853145

Modelling three-way catalytic converter oriented to engine cold-start conditions

Marcelo REAL[1], Raffael HEDINGER[2], Benjamín PLA[1], Christopher ONDER[2]

Abstract

This paper introduces a physical model of a three-way catalytic converter oriented to engine cold-start conditions. Computational cost is an important factor, particularly when the modelling is oriented to the development of engine control strategies. That is why a one-dimensional one-channel real-time capable model is proposed. The present model accounts for two phases, gas and solid respectively, considering not only the heat transfer by convection between both, but also the water vapour condensation and evaporation in the catalyst brick, which plays a key role during engine cold-start. Moreover, the model addresses the conductive heat flow, heat losses to the environment and exothermic reactions in the solid phase, as well as the convective heat flow in the gas phase. Regarding the chemical model, the oxidation of hydrocarbons and carbon monoxide is considered by means of the Langmuir-Hinshelwood mechanism. Three layers make up the model structure from a kinetic point of view, bulk gas, washcoat pores and noble metal in the catalyst surface. The model takes fuel-to-air ratio, exhaust gas mass flow, temperature, pressure and gas composition as inputs, providing the thermal distribution as well as the species concentration along the converter.

Keywords

Control-oriented modelling, Three-way catalyst, After-treatment systems, Catalyst warm-up, Engine cold-start

1 Introduction

Three-way catalytic converters (TWC) allow to oxidize hydrocarbons (HC) and carbon monoxide (CO) while reducing nitrogen oxides (NO_x) simultaneously, but only if the temperature is high enough. It means that during the first 40 to 100 seconds of the engine cold-start, a noticeable amount of pollutant species are emitted, particularly CO and HC. In fact, during this period the HC emissions represent a 60-80% of the total HC emitted in a regulatory test procedure[1–4]. This is not only a consequence of the low efficiency of TWC at low temperatures, but also of the incomplete combustion that takes place when the engine is below its working temperature[5–7]. Different approaches can be followed to deal with this issue, from using additional hardware components in order to heat-up faster the TWC[8–20], to developing specific control strategies like ignition retardation or homogeneous split mode injection, in order to not only heat-up the TWC faster but also reducing HC exhaust raw emissions[21–23]. Ignition retardation allows to delay the combustion process, thereby the combustion remains active even during the exhaust stroke, which helps to speed up the catalyst heating process. Nevertheless, keeping low HC emissions represents a challenge when high levels of ignition retardation are imposed. At this point, homogeneous split mode injection plays a key role, since it enables lean global mixtures but also ensures the ignition. In order to fulfil both requirements the fuel injection is split into two parts. First, a homogeneous lean charge is carried out during the intake stroke. Then, an additional amount of fuel is injected just before the ignition, providing a local rich mixture around the spark plug to ensure a proper ignition of the homogeneous lean charge[24,25].

Taking into account the low emissions level allowed by current legislation and the future zero emissions trends, the pollutant emissions reduction during cold-start phase is imperative. The development of the aforementioned control strategies needs reliable models to gain insight into the TWC behaviour. However, multi-dimensional, detailed, first-principle models[26–33] present excessive computational requirements for control purposes. Other first-principle models in the literature are one-dimensional evolutions of the previous ones, developed with the idea of reducing the computational demand[34–45]. But they often require a considerable amount of time to run simulations, and especially while properly identifying their parameters. Usually, because complex kinetic approaches are proposed, with a remarkable amount of chemical reactions[13,41,46]. On the other hand, lumped-parameter control-oriented models, some of them based on first principles and other ones gray or black-box models based on phenomenological correlations[47–58], are fast enough even for on-board applications, but usually their assumptions and simplifications of the physical phenomena do not allow to understand what is actually happening inside the converter.

It is not common to find a first-principle TWC model with low computational requirements, oriented to

[1]CMT-Motores Térmicos, Universitat Politècnica de València, 46022 Valencia, Spain

[2]Institute for Dynamic Systems and Control, ETH Zurich, 8092 Zurich, Switzerland

Corresponding author:

Marcelo REAL, Camino de Vera, s/n 46022 Valencia, Spain

Email: marreami@mot.upv.es

predict the converter behaviour under cold-start conditions, experimentally validated and which also takes into account water evaporation and condensation. Most of the models present in literature miss some of these features. The present paper aims to cover this room. In particular, the effect of water vapour condensation and evaporation is fundamental to properly predict the temperature evolution at the beginning of the catalyst heating up process. When the cold converter is fed with hot exhaust gases, the brick surface becomes wet due to the water vapour condensation. After some seconds, the heat transferred from the gas to the brick progressively increases the temperature on each longitudinal section from the inlet to the outlet, which involves the end of the water vapour condensation and the start of the evaporation. During the evaporation process, the temperature of the corresponding section remains constant. Then, the temperature of the dry section rises again pushed by the heat transfer from the exhaust gas. This process moves along the brick length and it can take more than 60 seconds, of course, depending on the exhaust gas mass flow and temperature. Meanwhile, the temperature in the inlet sections of the converter can be high enough to allow the start of the oxidation reactions, which in turn increases the heat available to evaporate the water condensed in the subsequent sections, thus speeding up the process.

This complex phenomenon leads the TWC behaviour during the heating up process, thereby a model capable of taking this issue into account is essential to help in the development of cold-start strategies. That is why a one-dimensional one-channel (hereinafter 1D-1Ch) scheme is proposed. The thermal model takes into account detailed heat transfer phenomena, including heat release of exothermic reactions as well as water evaporation and condensation. The kinetic reactions are also based on first principles, accounting for gas transfer between bulk gas and washcoat pores, as well as adsorption and desorption of species on noble metal coating in the catalyst surface. However, a simplified set of reactions is used to reduce the model complexity. The idea is to keep the model as simple as possible in order to preserve real-time capabilities. Only the sorption of all reactants as well as HC and CO oxidation are considered, since the model is oriented to aid in the development of engine control strategies during cold-start. That is why NOx reactions and oxygen storing in ceria are neglected. NOx raw emissions are expected to be low because of the retarded combustion imposed during cold-start[21]. While oxygen storing in ceria neither plays a crucial role during cold-start[49,50], particularly, if fuel-to-air ratio is kept at lean conditions to decrease HC and CO raw emissions[25].

The paper is organised as follows: a description of the tools and facilities used in order to carry out the experimental activities is detailed in section 2. Section 3 explains the model structure and describes the thermal and chemical phenomena included. The experimental validation of the model is shown in section 4. Finally, the conclusions of the present work are summarized in section 5. Additionally, a specific process to get a proper parameter identification is proposed in *Appendix A*.

2 Tools

All the data collected for the model fitting and validation have been obtained by means of experimental tests in the facilities of the Institute for Dynamic Systems and Control, ETH Zurich. The engine test bench is equipped with two fast analyzers to measure hydrocarbons (HC) and carbon monoxide (CO) at the inlet and outlet of the TWC, in particular, the analyzers Cambustion HFR400 and NDIR500 have been used respectively. Regarding the internal combustion engine, it is a turbocharged GDI engine representative of the current state of the art. The advantage of using a real engine to collect the required data lies in the fact that the TWC is exposed to an exhaust gas flow totally equivalent to the real driving conditions, i.e., with the same temperatures, mass flows, pulsed gas flow and exhaust gas composition, which is particularly relevant. Concerning the catalytic converter used, it is fully instrumented to measure temperature at several points longitudinally distributed inside the brick as well as pressure and fuel-to-air ratio at catalyst inlet.

3 TWC model description

This model has been created keeping in mind the idea of developing control strategies for the TWC warm-up. In this sense, this work focuses mostly on operating conditions before and during light-off. However, the current approach is not restricted to those conditions, since the model could be also used to simulate operating conditions after light-off, although in this case there is no water vapour condensation and evaporation.

The development of control strategies requires an important experimental effort to understand, assess and validate the results. The present model helps to partially reduce this experimental work by providing reliable estimations about thermal distribution as well as CO and HC emissions. In this sense, this is not a control-oriented model for on-board applications, but a model for off-line approaches. However, low computational requirements are always an advantage, particularly when complex strategies with hundreds of different cases must be checked. That is why the authors have restricted the model complexity, although always keeping the first-principle approach, with the aim of creating a model with real-time capabilities.

Furthermore, the model has been created with very specific purposes, since state-of-the-art cold-start strategies deal with particular operating conditions:

- TWC heating up process, that is, strong dependency between conversion efficiency and temperature.
- Atypical combustion due to retarded ignition and homogeneous split mode injection.
- Lean conditions to reduce as much as possible HC raw emissions.

As a consequence, the engine raw emissions have a very particular composition in comparison with normal operation, oxygen availability at catalyst inlet but low NOx emissions. In addition, phenomena such as the water condensation-evaporation that are usually neglected, play here a key role due to the cold conditions of the brick. In order to reduce

the actual complexity of the physical phenomena involved and fulfil the computational requirements, the following assumptions are made [13,35–37,41,57,59]:

- The exhaust gas and flow at catalyst inlet is uniform, that is, the concentration, temperature and velocity are the same for all particles within a cross section. Therefore, the gas velocity as well as the temperature and concentration gradients in the radial direction are neglected. Only axial gradients are considered. However, axial diffusion is not considered in the mass balance because its effect is negligible for the current approach.
- The metal loading in the brick converter is totally homogeneous. Moreover, all channels are impenetrable to gas and have the same diameter. Thus, the behaviour of any individual channel is representative of the entire monolith.
- The number of free vacancies in noble metal (catalyst surface) is constant and all of them are equivalent for all species considered.
- Once the gas is inside the channel, heat radiation and conduction as well as axial diffusion are neglected. Since the effect of convection due to the gas flow prevails over the other ones.
- The pressure drop along the channel is neglected, thereby the gas density is only a function of the temperature. The effect of the gas composition is not considered.
- The feed-stream is always lean, so oxygen storing dynamics in ceria are neglected.

These simplifications lead to develop a 1D-1Ch approach. The specific features and formulation are detailed in the next sub-sections. A further explanation regarding some particular aspects of catalyst modelling can be found in the literature [59]. The main geometrical specifications of the TWC are summarized in Table 1:

Table 1: TWC geometrical specifications	
Brick length:	0.18 m
Brick diameter:	0.12 m
Brick cell density:	400 cpsi

3.1 Thermal model

Two phases have been considered from the heat transfer point of view, the gas phase flowing along the channel and the solid phase that constitutes the walls of the aforementioned channel. A simplified diagram is shown in Figure 1.

The energy balance in the gas phase only accounts for two terms, the axial convection and the heat transfer between the gas and the solid phase, as it is shown in equation (1). The specific heat of the gas phase is the addition of two terms: the specific heat of the gas itself and the specific heat of the water vapour contained in the gas stream, weighted with the concentration of the water vapour.

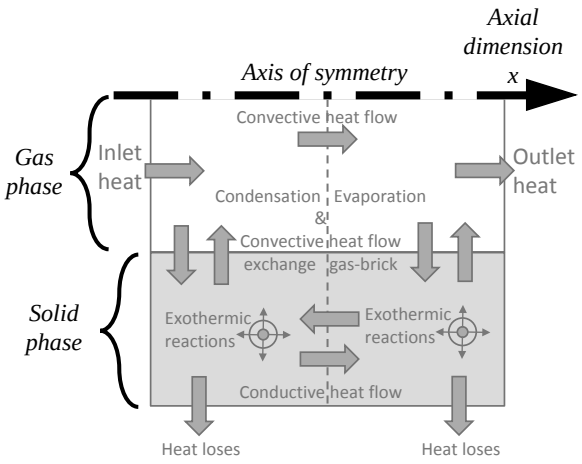

Figure 1. Heat transfer diagram of the 1D-1Ch model.

$$\varepsilon \cdot \varphi_g \cdot (c_g + X_w \cdot c_w) \cdot \frac{\partial T_g}{\partial t} = \\ = -\alpha \cdot a_v \cdot (T_g - T_{brick}) - \\ - \frac{\dot{m}_{exh}}{A} \cdot (c_g + X_w \cdot c_w) \cdot \frac{\partial T_g}{\partial x} \tag{1}$$

In the solid phase, the energy balance consists of five terms: axial conduction, heat transfer between gas and catalyst surface, latent heat of water vapour that condensates or evaporates in the monolith walls, heat losses to the environment and heat produced by the exothermic reactions (equation (2)).

$$(1-\varepsilon) \cdot \varphi_{brick} \cdot (c_{brick} + X_w \cdot c_w) \cdot \frac{\partial T_{brick}}{\partial t} = \\ = k_{brick} \cdot (1-\varepsilon) \cdot \frac{\partial^2 T_{brick}}{\partial x^2} + \alpha \cdot a_v \cdot (T_g - T_{brick}) + \\ + \delta \cdot \beta_i \cdot a_v \varphi_w \cdot (X_w - X_{w,sat}) \cdot \\ \cdot (\Delta H_{evap} + c_w \cdot (T_g - T_{brick})) + \\ + \alpha_{env} \cdot a_{v,env} \cdot (T_{brick} - T_{env}) + \\ + a_{cat} \cdot C \cdot \sum_{j=1}^{n} (-\Delta H_{r_j} \cdot r_j) \tag{2}$$

The water vapour condensation and evaporation phenomenon has been considered following the approach proposed in *Frauhammer et al.* [60]. The associated term is weighted with the non-linear function δ, which is zero except when there is water vapour condensation or evaporation.

3.2 Reaction scheme

Three layers make up the structure of the chemical model considered, as it is shown in Figure 2. In the same way that happens with the structure of the heat transfer model, the outer layer corresponds to the gas that flows inside the channel.

In the gas phase, the mass balance of each species considered (i) consists of only two terms (equation (3)), the mass transfer between gas and washcoat pores as well as the convective flow. Axial diffusion is neglected in this approach.

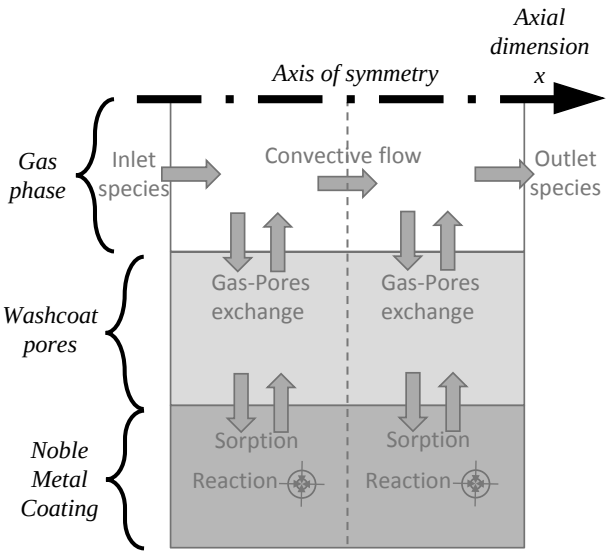

Figure 2. Kinetic diagram of the 1D-1Ch model.

$$\varepsilon \cdot A \cdot \varphi_g \cdot \frac{\partial X_i}{\partial t} = \\ = -\beta_i \cdot A \cdot a_v \cdot \varphi_g \cdot (X_i - Y_i) - \dot{m}_{exh} \cdot \frac{\partial X_i}{\partial x} \quad (3)$$

In the particular case of water vapour (equation (4)), the main difference is that the mass transfer term does not depend on the concentration in the solid phase (Y_i), but on the maximum concentration allowed under saturation conditions ($X_{w,sat}$) in the gas phase.

$$\varepsilon \cdot \varphi_g \cdot \frac{\partial X_w}{\partial t} = \\ = -\beta_w \cdot \delta \cdot a_v \cdot \varphi_g \cdot (X_w - X_{w,sat}) - \frac{\dot{m}_{exh}}{A} \cdot \frac{\partial X_w}{\partial x} \quad (4)$$

The washcoat pores constitute the second layer of the chemical model. It behaves as an interface between gas and catalyst surface, which in turn is the third layer and the innermost of the chemical model. Here, the species are adsorbed prior to react with the aid of the noble metal coating. Thereby, all the reactions considered follow the Langmuir-Hinshelwood mechanism. The mass balance of each species in the washcoat pores also consists of two terms (equation (5)), the mass transfer between gas and pores as well as the mass production term. The latter acts like a sink or a source depending on whether the species are being adsorbed or desorbed respectively. There is no mass transfer in axial direction within the solid phase, thus the mass transport along the catalyst is limited to the gas phase. For water vapour, the differences are analogous to those mentioned in the gas phase.

$$4 \cdot d_b \cdot d_w \cdot \varepsilon_{washcoat} \cdot \varphi_g \cdot \frac{\partial Y_i}{\partial t} = \\ = \beta_i \cdot A \cdot a_v \cdot \varphi_g \cdot (X_i - Y_i) - \\ - a_{cat} \cdot C \cdot A \cdot \sum_{j=1}^{n} (r_j \cdot v_{i,j} \cdot M_i) \quad (5)$$

In the third layer, assuming that all vacancies are equivalent, the mass balance (equation (6)) of species adsorbed and desorbed (as well as the free vacancies) in the noble metal coating, consists of as many terms as reactions (j) in which the considered species (i) takes part.

$$\frac{\partial \Theta i}{\partial t} = \sum_{j=1}^{k} v_{i,j} \cdot r_j \quad (6)$$

Only 5 reactions are considered (equations (7)-(11)). Carbon monoxide as well as hydrocarbons adsorption and desorption are taken into account. For simplicity, the oxidation of HC is lumped in just one reaction: propylene (C_3H_6), which usually represents the predominant and easily oxidizing HC[44]. Regarding oxygen, only its adsorption is modelled, the desorption is carried out by means of CO and HC oxidation. As mentioned previously, the reaction that considers the reduction of NOx with CO has been omitted because low NOx exhaust raw emissions are expected under very retarded ignition conditions. Pt represents the vacant sites of noble metal on which the gaseous species can be adsorbed, while Pt- represents the vacancies occupied by the corresponding species.

$$O_2 + 2Pt \rightarrow 2PtO \quad (7)$$
$$CO + Pt \leftrightarrows PtCO \quad (8)$$
$$C_3H_6 + Pt \leftrightarrows PtC_3H_6 \quad (9)$$
$$PtCO + PtO \rightarrow CO_2 + 2Pt \quad (10)$$
$$PtC_3H_6 + 9PtO \rightarrow 3CO_2 + 3H_2O + 10Pt \quad (11)$$

Forward reaction-rate constants follow the Arrhenius equation (12) in the case of oxidation reactions, or the sticking equation (13) in the case of adsorption reactions.

$$k_j^f = A_j \cdot exp\frac{-E_{a_j}}{R \cdot T_{brick}} \quad (12)$$

$$k_j^f = \frac{1}{C} \cdot \frac{s_i}{\sqrt{2 \cdot \pi \cdot M_i \cdot R \cdot T_g}} \quad (13)$$

According to the model structure, it consists of 13 states: temperatures of gas and solid phases (T_g and T_{brick} respectively); water, oxygen, carbon monoxide and hydrocarbons concentration in both gas and washcoat pores (X_i and Y_i respectively); and vacancies occupied by all adsorbed species in the noble metal coating of the catalyst surface (Θ_i). All the model states are summarized in the state vector S:

$$S = \begin{bmatrix} T_g \\ T_{brick} \\ X_{CO} \\ X_{O_2} \\ X_{HC} \\ X_w \\ Y_{CO} \\ Y_{O_2} \\ Y_{HC} \\ Y_w \\ \Theta_{CO} \\ \Theta_{O_2} \\ \Theta_{HC} \end{bmatrix} \quad (14)$$

3.3 Numerical solution

The present 1D-1Ch approach requires solving a partial differential equations (PDE) system. It is solved discretizing the problem with the finite differences method (FDM), in particular, the Euler forward method is chosen for first-order temporal derivatives. For the spatial discretization of first-order derivatives, backward differences are used, while the spatial second-order derivative (imposed by the thermal conduction term) is discretized with central differences. Concerning the boundaries, Dirichlet conditions are imposed in spatial and temporal first-order discretizations, since the inlet values of gas concentration, temperature and exhaust mass flow are known, as well as the temporal solution of the previous step. Neumann boundary conditions are set for the spatial second-order derivative, that is, null conductive heat flow at the inner and outer sections of the solid phase (equation (15)).

$$\frac{\partial T_{brick}(0,t)}{\partial x} = \frac{\partial T_{brick}(L,t)}{\partial x} = 0, \quad x \in [0, L] \qquad (15)$$

Since relatively low air mass flow is expected under cold-start conditions, the spatial discretization is set to 10 mm, while the temporal discretization is 1 ms. Defining the real-time ratio as the elapsed time to perform a simulation divided by the duration of the simulation, the present approach runs at 0.35 s/s, thus, in real-time. The processor used for such rating is an Intel® Core™ i5-4460 @ 3.2 GHz. The authors consider that the model is fast enough for the required off-line tasks.

4 Experimental validation

Several validation tests are shown next. The simulation results provide information experimentally non-measurable that helps to gain insight into the TWC behaviour during cold-start, which is in fact one of the model purposes.

Figures 3 and 4 show the results provided by the model during a cold-start test at idling, with the engine speed set to 1200 rpm. As a consequence of the high ignition retardation (the center of combustion is set to 100 CA degrees ATDC) as well as to the lean fuel-to-air equivalence ratio imposed (0.95), the combustion efficiency is low, thus a mass flow of 26 kg/h is needed to avoid stalling. The transient from 0 to 1200 rpm takes 1 second, while other operating parameters, as fuel-to-air ratio or center of combustion need 4 seconds to reach steady conditions (basically the time needed by the λ-sensor to provide a reliable measurement). These particular operating conditions are part of a cold-start strategy proposed in the literature[25].

At the very beginning, both the gas and the converter are at ambient temperature, thus the water content of the exhaust stream begins to condensate in the catalyst surface, particularly in the front face of the brick. After five seconds, the inlet gas temperature increases, which heats up the first centimetres of the brick. This temperature increase involves the end of the water condensation in the front face of the catalyst and the starting of the evaporation. The subsequent sections of the brick are warmer than environment but still cold, thus the inlet water vapour along with the water evaporated in the first sections tend to condensate

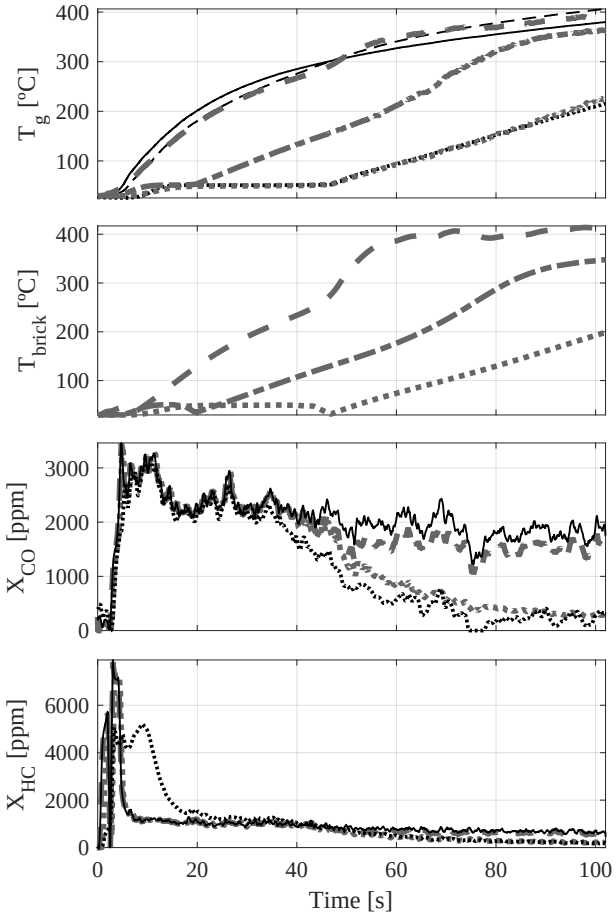

Figure 3. Air mass flow equal to 26 kg/h. Temperatures and emissions evolution. Black lines represent experimental data while gray lines are model predictions. Solid (——), dashed (- - -), dash-dot (-·-·-) and dotted (·····) lines correspond to inlet, first section, central section and outlet respectively.

progressively on them. After seven seconds, the inlet brick sections are completely dry. In these sections gas and catalyst temperature increase strongly following the inlet temperature profile with a small delay, while the temperature in the brick sections that are still wet is kept at 50 °C.

The conversion of species is zero during the first 40 seconds, so inlet and outlet concentrations are almost identical for CO. However, during first 15 seconds HC emissions behaves in a different way according to the experimental measurements. It seems that at the very beginning of the cold-start the catalyst is able to store HC, since the concentration at the inlet is higher than at the outlet. However, a few seconds later the behaviour is the opposite. The explanation for this phenomenon could be based on the fact that not only water but also HC condensates in the catalyst surface. Of course the model is not able to represent such behaviour, since only water vapour condensation is taken into account. Anyway, from the emissions point of view, this behaviour is negligible because these HC are not being converted, only stored and released within the first 15 seconds of the cold-start.

After 40 seconds, the front sections of the brick reach the lower threshold of the conversion temperature (240 °C). Because of that, tailpipe CO emissions begin to decrease. Activation energy for HC oxidation is slightly higher, thus

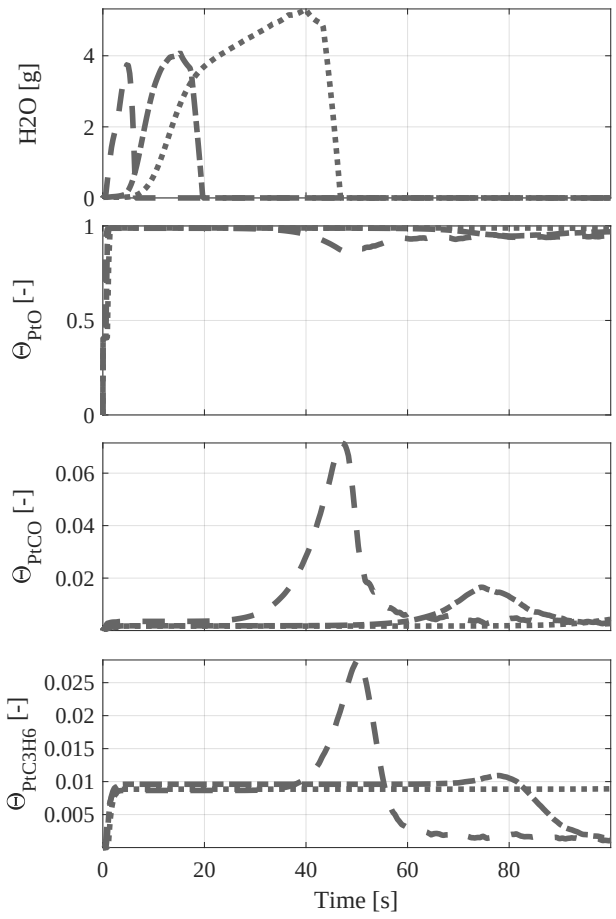

Figure 4. Air mass flow equal to 26 kg/h. Model predictions for water content and sites occupied by the species adsorbed in noble metal. Dashed (- - -), dash-dot (-·-·) and dotted (·····) lines correspond to first section, central section and outlet respectively.

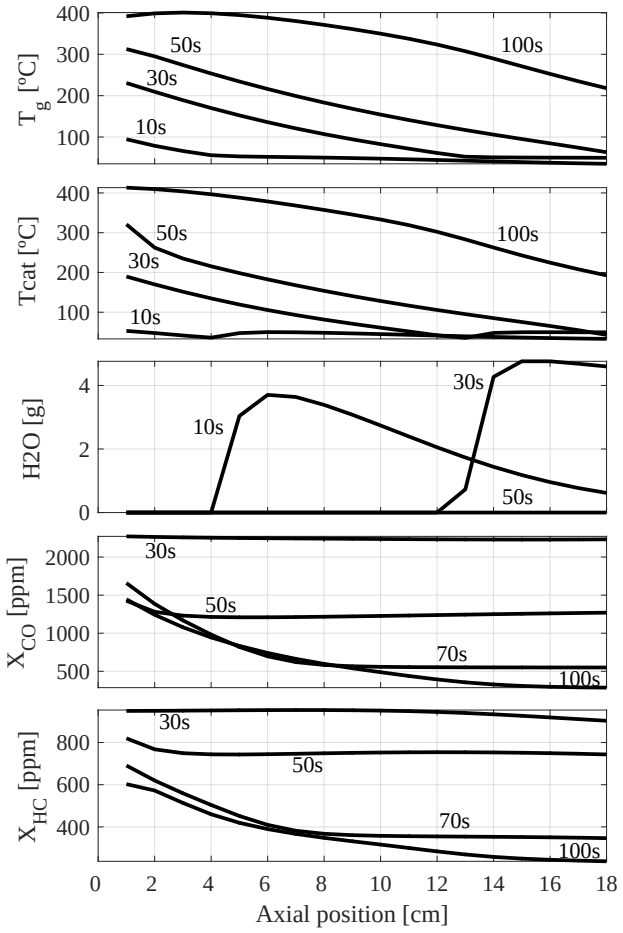

Figure 5. Air mass flow equal to 26 kg/h. Model predictions for temperatures, water content and emissions distribution along the TWC axis.

their conversion begin later. This start of conversion involves a change in the heat transfer phenomenon, until this moment the inlet gas was heating the brick, but from second 40 on, the exothermic reaction of CO oxidation is heating the first brick sections. Figure 5 shows this evolution based on the catalyst length for the same test as the previous figures.

The parameter identification indicates that conductive heat flow is negligible in solid phase, which is reasonable, since the heat conduction coefficient of the ceramic is low. Furthermore, the heat transfer surface is very small due to the thin brick walls. However, exothermic reactions not only heat up the sections at which the reaction is taking place, but also the following ones. It is due to the heat exchange between gas and brick together with the conductive heat flow in gas phase, that drags the reactions heat. According to the model, the temperature at the front face of the converter rises from 240 to 340 °C in 12 seconds (from 40 to 52 s), surpassing the inlet gas temperature (first and second plot of Figure 3). The experimental measurements corroborates the model estimation, since gas temperature in the first section of the converter also exceeds the inlet gas temperature from second 46 onward. By then, the whole brick is dry, as all water vapour has been evaporated. The model simulation matches with the experimental data regarding the duration of the plateau for the outlet temperature. Both heat sources have contributed to this fact, the inlet heat as well as the heat of the exothermic reactions.

In the noble metal coating, the vacancies occupied by the different species show that the TWC is mostly filled with oxygen during the whole test (Figure 4) as expected, since lean fuel-to-air ratio is applied. The percentage of vacancies occupied by CO and HC reaches its maximum just before the beginning of the oxidation reactions, again some seconds earlier for CO than for HC. After 100 seconds, the conversion efficiency is high for both species considered. However, due to the relatively low air mass flow, only the first two thirds of the catalyst length are above light-off temperature (Figure 5). The evolution of the emissions shows how most of the oxidation takes place in the first 10 centimetres. The temperature of the brick also corroborates this fact, since only the first half of the converter's length shows a change of slope in the temperature profiles (Figure 3). Figures 6 and 7 show similar cold-start tests with different air mass flows, 21 and 18 kg/h respectively. As a consequence of the mass flow decrease, the duration of the plateau for the outlet temperature increases. The model is able to predict this phenomenon, where water condensation and evaporation play a key role, as well as the consequent emissions decrease.

The error distribution for temperature, CO and HC emissions at catalyst outlet in the three tests shown previously is summarized in Figure 8. The x-axis represents

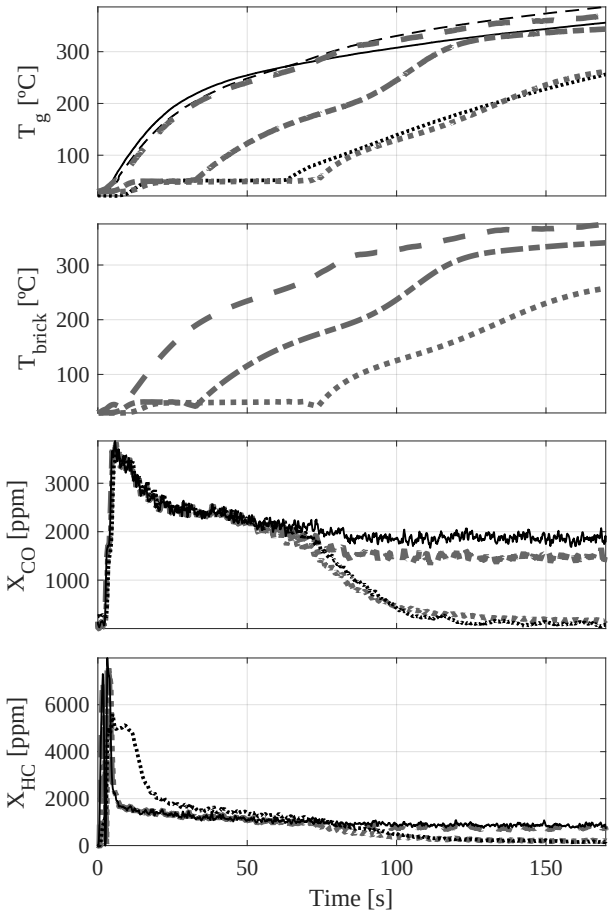

Figure 6. Air mass flow equal to 21 kg/h. Temperatures and emissions evolution. Black lines represent experimental data while gray lines are model predictions. Solid (——), dashed (- - -), dash-dot (-·-·) and dotted (·····) lines correspond to inlet, first section, central section and outlet respectively.

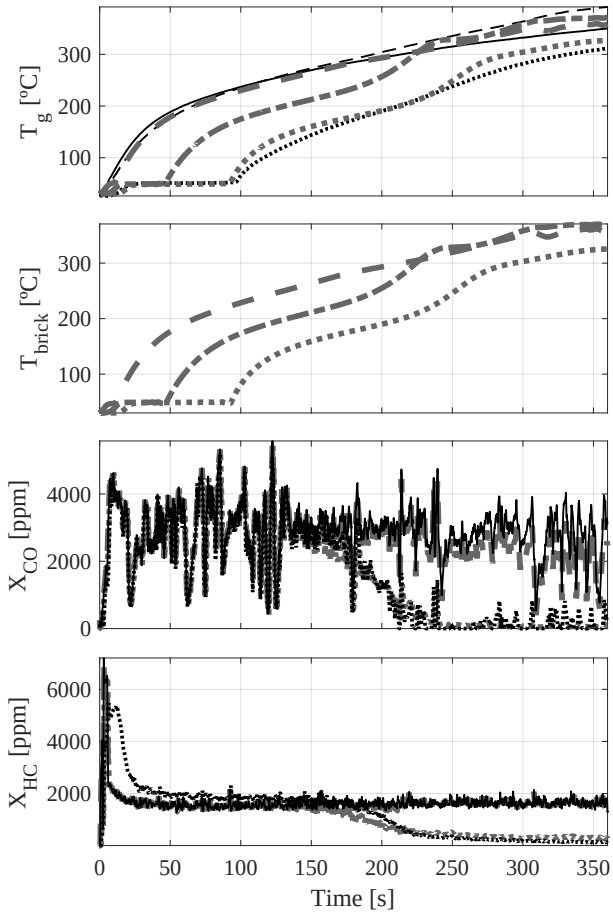

Figure 7. Air mass flow equal to 18 kg/h. Temperatures and emissions evolution. Black lines represent experimental data while gray lines are model predictions. Solid (——), dashed (- - -), dash-dot (-·-·) and dotted (·····) lines correspond to inlet, first section, central section and outlet respectively.

the percentage of samples with an error below a certain threshold, while the y-axis represents the corresponding value of the error for each parameter assessed. In particular, during the simulation the 90 % of the samples have an error in the outlet temperature below 23 degrees, as well as below 408 an 212 ppm in the case of CO and HC emissions respectively. The highest errors in terms of emissions correspond to the first seconds of the tests, when the inlet gas composition changes fast as a consequence of the engine start-up, as well as to the aforementioned HC condensation.

In Figure 9 a double step in air mass flow is performed. It reaches 40 kg/h until second 27, then decreases fast until 16 kg/h. Finally, the air mass flow increases again until 29 kg/h at second 50 and it is kept at steady conditions until the end of the test. As a consequence of these changes, the plateau of the outlet temperature is not so well defined, and the model overestimates the outlet temperature. However, the emissions prediction is still good because that temperature is not driving the species conversion, but the temperatures of the front sections. A zero-dimensional model would fail if that happens. In contrast to previous tests, the air mass flow evolution involves the change of the slope at the inlet temperature. Both the inlet temperature as well as the temperature in the first section of the converter reach a value above 400 °C before decreasing again to 300 °C.

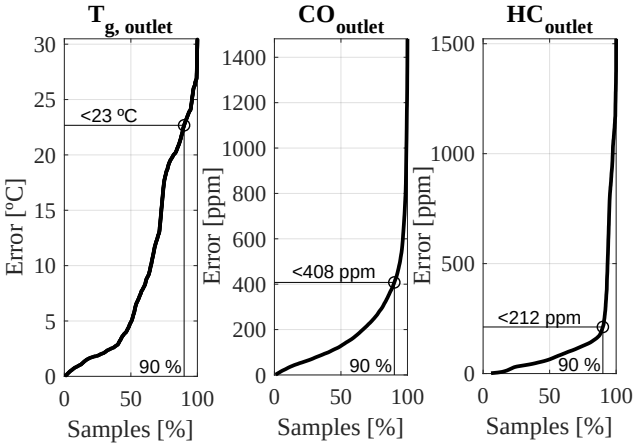

Figure 8. Error distribution for temperature, CO and HC emissions at catalyst outlet in the three tests shown previously with air mass flows equal to 26, 21 and 18 kg/h respectively.

The HC conversion is affected by this temperature reduction showing a peak in emissions. However, this is not the case of CO emissions because of its lower activation energy. The model is also able to predict that peak, although the slight temperature overestimation anticipates the aforementioned emissions increase.

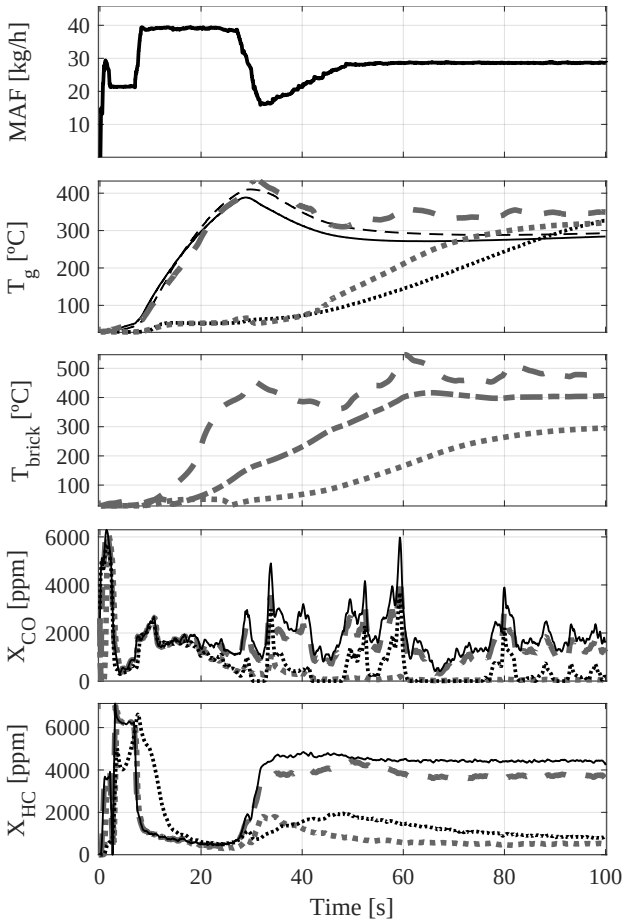

Figure 9. Test with air mass flow steps. Temperatures and emissions evolution. Black lines represent experimental data while gray lines are model predictions. Solid (——), dashed (- - -), dash-dot (-·-·) and dotted (·····) lines correspond to inlet, first section, central section and outlet respectively.

5 Summary and conclusions

State-of-the-art approaches for catalyst warm-up during engine cold-start tend to take advantage of direct injection systems in order to operate with very retarded ignition, thanks to homogeneous split mode injection. Because of the atypical combustion imposed and the low in-cylinder temperatures, the TWC has to deal with very particular exhaust gas composition, like oxygen availability but low NOx, and important amounts of HC and CO. The condensation of water vapour on the catalyst surface is usually neglected in TWC modelling, but under the aforementioned conditions its consideration is indispensable to properly simulate the catalyst behaviour. As a consequence of the catalyst heating-up process, there is also a strong coupling between catalyst temperatures and conversion efficiency. To deal with all these requirements, a first-principle, 1D-1Ch TWC model oriented to aid in the development of engine control strategies for cold-start conditions has been presented.

Water vapour condensation and evaporation are fundamental for the understanding of the TWC behaviour at the very beginning of the heating-up process, since the thermal dynamics during first minutes are driven by this phenomenon. Under this conditions the catalyst temperature evolution exhibits a plateau due to the water evaporation, the developed model is able to represent this evolution along the TWC accurately, and also provides useful estimations for CO and HC emissions. According to the results obtained, probably not only water but a mix of water vapour and HC is condensing at the very beginning of the cold-start. Future works could improve the model capabilities by considering the condensation of different species.

Although the conductive heat flow in solid phase is included in the model, the parameter identification process shows that it could be neglected. According to the authors' point of view, this result is coherent with the typical low conduction capabilities of ceramic materials, as well as with the small heat transfer surface, due to the extremely thin brick walls. This fact can be taken into account for future model updates, simplifying the the complexity and speeding up the model.

Appendix A: Parameter identification

It is not easy to find in the literature details about how tuning the wide variety of existing catalyst models. Partly because the proper model fitting process strongly depends on the variety and amount of experimental information available, as well as on the type of model used. Despite these difficulties, some authors have provided general guidelines for this purpose[61]. In this sense, the current section proposes an specific iterative method for the developed model. Although it can be also taken as a general guide for similar models. Some of the parameters can be known if detailed data sheet of the TWC is available, as it is not always the case, the proposed method is based on the assumption that most of them are unknown.

This method consists of four steps, each one is oriented to obtain a different set of parameters by using a particular experimental test and cost function. The order is based on the need to use the parameters obtained with the previous step in the next step.

- *Step 0:* allows to obtain a first estimation of thermal parameters: β_{H_2O}, k_{brick}, α, α_{env} and c_{brick}. The use of experimental tests with a non-impregnated TWC is proposed.
- *Step 1:* allows to obtain the kinetic and chemical parameters: β_{O_2}, β_{CO}, $\beta_{C_3H_6}$, $\varepsilon_{washcoat}$, C, s_{O_2}, s_{CO}, $s_{C_3H_6}$, a_{cat}, k^b_{CO} and $k^b_{C_3H_6}$. Experimental tests with an already warmed catalyst (above light-off temperature) but with low heat generation due to exothermic reactions are recommended.
- *Step 2:* allows to obtain the Arrhenius coefficients: A_{CO}, $A_{C_3H_6}$, $E_{a,CO}$ and E_{a,C_3H_6}. Experimental tests with the whole evolution of the catalyst heating up process but still with lower requirement of heat generation.
- *Step 3:* allows to obtain the reaction enthalpies ($\Delta H_{r_{CO}}$ and $\Delta H_{r_{C_3H_6}}$) for the first time, and also to update the thermal parameters obtained in *Step 0*. Experimental tests with high heat generation are required.

In order to clarify the aforementioned process, a detailed explanation of each step can be found next.

Step 0: preliminary estimation of thermal parameters

First, the reaction enthalpy is set to zero for both CO and C_3H_6 oxidation reactions, therefore, the exothermic reactions heat are neglected. The appropriate experimental test would be a cold-start with a non-impregnated catalyst. If this hardware is not available, any test with low heat generation could be useful. By using any non-linear programming (NLP) or optimization solver, the preliminary values of the parameters that drive the model heat transfer can be identified: water vapour mass transfer coefficient (β_{H_2O}), heat transfer conduction coefficient (k_{brick}), heat transfer convection coefficient between gas and solid phase (α), heat losses convection coefficient (α_{env}) and specific heat capacity of the solid phase (c_{brick}). The cost function should provide information of, at least, inlet and outlet temperature errors, although any additional intermediate measurement is valuable.

Step 1: kinetics and chemical reaction parameters

Still neglecting the reaction enthalpies but once obtained a first estimation of the thermal parameters, the parameters related to the chemical reactions and the species mass transfer can be identified. Pre-exponential factors and activation energies of Arrhenius equations are still unknown, but they can be taken from the literature as first approach. Experimental tests with at least, inlet temperature and exhaust mass flow, O_2, CO and HC concentrations upstream and downstream of the TWC are needed (again, intermediate measurements would be valuable) to feed the cost function. In this case, operating conditions with TWC temperature above light-off are desirable, since Arrhenius parameters are just an estimation at this stage. However, tests with low heat generation due to exothermic reactions are still needed, because the reaction enthalpies are equal to zero by now. A NLP solver fed with a predefined cost function can provide the first estimation of the following parameters: O_2, CO and C_3H_6 mass transfer coefficients (β_{O_2}, β_{CO} and $\beta_{C_3H_6}$), washcoat porosity ($\varepsilon_{washcoat}$), maximum capacity of adsorbed species (C), fraction of collisions actually leading to O_2, CO and C_3H_6 adsorption reactions (s_{O_2}, s_{CO} and $s_{C_3H_6}$), relative catalytically active area per catalyst volume (a_{cat}), and backward coefficients for CO and C_3H_6 desorption reactions (k^b_{CO} and $k^b_{C_3H_6}$).

Step 2: Arrhenius coefficients

Imposing the parameters identified in previous steps and neglecting the reaction enthalpies again, the pre-exponential factors (A_{CO} and $A_{C_3H_6}$) along with the activation energies ($E_{a,CO}$ and E_{a,C_3H_6}) of the Arrhenius equation can be updated. In this case, the proper experimental test must include the whole evolution of the catalyst heating up process from cold conditions, but still a heat of exothermic reactions as low as possible is desirable. Therefore, at least inlet temperature and exhaust mass flow, besides O_2, CO and HC concentrations upstream and downstream of the TWC are required. The cost function must provide information regarding the error in CO and HC emissions, at least at the catalyst outlet.

Step 3: thermal parameters

This is the last step of the first iteration. At this stage an initial estimation of all parameters, except the reaction enthalpies ($\Delta H_{r_{CO}}$ and $\Delta H_{r_{C_3H_6}}$), is available. For the first time, the experimental tests used to identify the parameters require high heat generation from the oxidation of CO and HC. Of course, including the whole evolution of the catalyst heating up process from cold conditions is more beneficial than tests with the TWC already heated up. All the thermal parameters estimated at *Step 0* together with the reaction enthalpies can be updated now. The cost function used to feed the NLP solver must provide information of, as least, the outlet temperatures, although intermediate temperature profiles can also be useful.

Once *Step 3* is completed, additional iterations from *Step 1* can be done until reaching the parameter convergence. The only difference is that, from the first iteration on, it is not necessary to neglect the reaction enthalpies. Which means that the experimental tests used in all steps can include the complete evolution of the catalyst heating up process without limitations regarding heat of exothermic reactions.

Appendix B: Nomenclature

i		Sub-index that takes into account the species considered
j		Sub-index that takes into account the reactions considered
w		Sub-index that represents the water vapour considered
ε	$[-]$	Volume fraction of the catalyst filled with gas
φ_g	$\left[\frac{kg}{m^3}\right]$	Exhaust gas density
c_g	$\left[\frac{J}{kgK}\right]$	Specific heat of the exhaust gas
X_w	$[-]$	Mass fraction of water vapour in gas phase
c_w	$\left[\frac{J}{kgK}\right]$	Specific heat of the gas
T_g	$[K]$	Gas temperature
t	$[s]$	Time
x	$[m]$	Axial dimension
α	$\left[\frac{J}{sKm^2}\right]$	Heat-transfer coefficient by convection between solid and gas phase
a_v	$\left[\frac{m^2}{m^3}\right]$	Relative cross-sectional surface
T_{brick}	$[K]$	Catalyst brick temperature
$\dot{m}_{exh}$	$\left[\frac{kg}{s}\right]$	Exhaust gas mass flow
A	$[m^2]$	Channel cross-section surface
φ_{brick}	$\left[\frac{kg}{m^3}\right]$	Catalyst brick density
c_{brick}	$\left[\frac{J}{kgK}\right]$	Specific heat of the catalyst brick
k_{brick}	$\left[\frac{J}{sKm}\right]$	Heat conduction coefficient of the solid phase
δ	$[-]$	Switch to enable or disable water vapour condensation-evaporation
β_i	$\left[\frac{m}{s}\right]$	Mass transfer coefficient
φ_w	$\left[\frac{kg}{m^3}\right]$	Water vapour density
$X_{w,sat}$	$[-]$	Saturation threshold for water vapour mass fraction in gas phase

ΔH_{evap}	$\left[\frac{J}{kg}\right]$	Water evaporation enthalpy
α_{env}	$\left[\frac{J}{sKm^2}\right]$	Heat-transfer coefficient by convection between solid and environment
$a_{v,env}$	$\left[\frac{m^2}{m^3}\right]$	Relative surface of heat losses
T_{env}	$[K]$	Environment temperature
a_{cat}	$\left[\frac{m^2}{m^3}\right]$	Relative catalytically active surface per catalyst volume
L	$[m]$	Catalyst brick length
C	$\left[\frac{mol}{m^2}\right]$	Maximum capacity of adsorbed species
ΔH_{r_j}	$\left[\frac{J}{mol}\right]$	Reaction enthalpy
r_j	$\left[s^{-1}\right]$	Reaction rate
k_j^f	$\left[s^{-1}\right]$	Forward reaction-rate constant
s_i	$[-]$	Sticking probability
M_i	$\left[\frac{kg}{mol}\right]$	Molecular mass
A_j	$\left[s^{-1}\right]$	Pre-exponential factor of Arrhenius law
Ea_j	$\left[\frac{J}{mol}\right]$	Activation energy of Arrhenius law
R	$\left[\frac{J}{molK}\right]$	Universal gas constant
X_i	$[-]$	Mass fraction of species in gas phase
Y_i	$[-]$	Mass fraction of species in solid phase
d_b	$[m]$	Channel side length
d_w	$[m]$	Washcoat thickness
$\varepsilon_{washcoat}$	$[-]$	Washcoat porosity
$v_{i,j}$	$[-]$	Stoichiometric factor
Θ_i	$[-]$	Fraction of sites in the noble metal coating occupied by the species i
S	$[-]$	State vector

Funding

This work was developed during the research stay of Marcelo Real at ETH Zurich, supported by the *Programa de Movilidad para la Formación de Personal Investigador del Vicerrectorado de Investigación, Innovación y Transferencia de la UPV*.

References

1. Shelef M and McCabe RW. Twenty-five years after introduction of automotive catalysts: what next? *Catalysis today* 2000; 62(1): 35–50.
2. Paul D. *Automobiles and pollution*. Warrendale PA. USA: SAE: Inc, 1995.
3. European commission Joint Research Centre: Geneva, Switzerland. *Regulated emissions of a Euro 5 passenger car measured over different driving cycles*, 2010.
4. Araki M, Sakairi K, Kuribara T et al. Effects of injection parameters on the amount of wall-wet fuel in a port-fuel-injected spark-ignition engine during cold start. *International Journal of Engine Research* 2019; DOI:10.1177/1468087419837768.
5. Gao J and Kuo TW. Toward the accurate prediction of soot in engine applications. *International Journal of Engine Research* 2018; DOI:10.1177/1468087418773937.
6. Guardiola C, Pla B, Bares P et al. An on-board method to estimate the light-off temperature of diesel oxidation catalysts. *International Journal of Engine Research* 2018; DOI:10.1177/1468087418817965.
7. Baron JH and Cheng WK. Back pressure effect on three-way catalyst light-off. *International Journal of Engine Research* 2018; DOI:10.1177/1468087418779505.
8. Yaegashi T, Yoshizaki K, Nagami T et al. New technology for reducing the power consumption of electrically heated catalysts. *SAE transactions* 1994; : 95–102.
9. Glander D and Zidat S. Mathematical modeling of electrically heated monolith converters: meeting european emissions regulations proposed for 2000 and 2005. Technical Report No. 972852, SAE Technical Paper, 1997.
10. Oh SH, Bissett EJ and Battiston PA. Mathematical modeling of electrically heated monolith converters: model formulation, numerical methods, and experimental verification. *Industrial & engineering chemistry research* 1993; 32(8): 1560–1567.
11. Katashiba H, Nishiyama R, Nishimura Y et al. Development of an effective air-injection system with heated air for lev/ulev. Technical Report No. 950411, SAE Technical Paper, 1995.
12. Kollmann K, Abthoff J, Zahn W et al. Secondary air injection with a new developed electrical blower for reduced exhaust emissions. Technical Report No. 940472, SAE Technical Paper, 1994.
13. Balenovic M, Hoebink J, Backx A et al. Modeling of an automotive exhaust gas converter at low temperatures aiming at control application. Technical Report (No. 1999-01-3623), SAE Technical Paper, 1999.
14. Takatsu K, Kurogi F, Matsue A et al. Dielectric heating catalytic converter system for reducing cold-start emissions. Technical Report No. 960344, SAE Technical Paper, 1996.
15. Pfalzgraf B, Otto E, Wirth A et al. The system development of electrically heated catalyst (ehc) for the lev and eu-iii legislation. *SAE transactions* 1995; : 777–787.
16. Heimrich MJ, Albu S and Osborn J. Electrically-heated catalyst system conversions on two current-technology vehicles. *SAE transactions* 1991; : 231–251.
17. Küper PF, Maus W, Swars H et al. Ultra-low power electrically-heated catalyst system. Technical Report No. 940465, SAE Technical Paper, 1994.
18. Socha LS and Thompson DF. Electrically heated extruded metal converters for low emission vehicles. Technical Report No. 920093, SAE Technical Paper, 1992.
19. Lee D and Heywood JB. Effects of secondary air injection during cold start of si engines. *SAE International Journal of Engines* 2010; 3(2): 182–196.
20. Pfahl U, Schatz A and Konieczny R. Advanced exhaust gas thermal management for lowest tailpipe emissions-combining low emission engine and electrically heated catalyst. Technical Report No. 2012-01-1090, SAE Technical Paper, 2012.
21. Chan S and Zhu J. The significance of high value of ignition retard control on the catalyst lightoff. Technical Report No. 962077, SAE Technical Paper, 1996.
22. Rodriguez JF and Cheng WK. Effect of operation strategy on first cycle co, hc, and pm/pn emissions in a gdi engine. *SAE International Journal of Engines* 2015; 8(3): 1098–1106.
23. Kimura K, Mori S, Kawauchi M et al. An investigation for reducing combustion instability under cold-start condition of a direct injection gasoline engine. *International Journal of Engine Research* 2019; 20(4): 470–479. DOI:10.1177/1468087418766924.
24. Reif K. *Gasoline Engine Management*. Friedrichshafen: Springer Vieweg, 2015.

25. Hedinger R, Elbert P and Onder C. Optimal cold-start control of a gasoline engine. *Energies* 2017; 10(10): 1548.
26. Yang H, Shu G, Tian H et al. Optimization of thermoelectric generator (teg) integrated with three-way catalytic converter (twc) for harvesting engine's exhaust waste heat. *Applied Thermal Engineering* 2018; 144: 628–638.
27. Irwin K, Douglas R, Stewart JD et al. Modelling the variation in precious metal dispersion in a three way catalytic converter after aging. Technical Report (No. 2018-01-0959), SAE Technical Paper, 2018.
28. Zygourakis K. Transient operation of monolith catalytic converters: a two-dimensional reactor model and the effects of radially nonuniform flow distributions. *Chemical Engineering Science* 1989; 44(9): 2075–2086.
29. Braun J, Hauber T, Többen H et al. Three-dimensional simulation of the transient behavior of a three-way catalytic converter. Technical Report No. 2002-01-0065, SAE Technical Paper, 2002.
30. Chen DK, Bissett EJ, Oh SH et al. A three-dimensional model for the analysis of transient thermal and conversion characteristics of monolithic catalytic converters. *SAE transactions* 1988; : 177–189.
31. Byrne H and Norbury J. Mathematical modelling of catalytic converters. *Mathematical engineering in industry* 1993; 4(1): 27–48.
32. Baba N, Ohsawa K and Sugiura S. Numerical approach for improving the conversion characteristics of exhaust catalysts under warming-up condition. Technical Report No. 962076, SAE Technical Paper, 1996.
33. Konstantas G and Stamatelos A. Modelling three-way catalytic converters: an effort to predict the effect of precious metal loading. *Proceedings of the Institution of Mechanical Engineers, Part D: Journal of Automobile Engineering* 2007; 221(3): 355–373.
34. Gong J, Wang D, Li J et al. An experimental and kinetic modeling study of aging impact on surface and subsurface oxygen storage in three-way catalysts. *Catalysis Today* 2017; .
35. Bickel J, Odendall B, Eigenberger G et al. Oxygen storage dominated three-way catalyst modeling for fresh catalysts. *Chemical Engineering Science* 2017; 160: 34–53.
36. Rink J, Meister N, Herbst F et al. Oxygen storage in three-way-catalysts is an equilibrium controlled process: Experimental investigation of the redox thermodynamics. *Applied Catalysis B: Environmental* 2017; 206: 104–114.
37. Sabatini S, Gelmini S, Hoffman MA et al. Design and experimental validation of a physics-based oxygen storage—thermal model for three way catalyst including aging. *Control Engineering Practice* 2017; 68: 89–101.
38. Gong J, Wang D, Li J et al. Dynamic oxygen storage modeling in a three-way catalyst for natural gas engines: A dual-site and shrinking-core diffusion approach. *Applied Catalysis B: Environmental* 2017; 203: 936–945.
39. Nievergeld AJL. *Automotive exhaust gas conversion: reaction kinetics, reactor modelling and control*. PhD Thesis, Technical University of Eindhoven, Eindhoven, The Netherlands, 1998.
40. Harmsen JMA. *Kinetic modelling of the dynamic behaviour of an automotive three-way catalyst under cold-start conditions*. PhD Thesis, Technische Universiteit Eindhoven, Eindhoven, The Netherlands, 2001.
41. Auckenthaler TS, Onder CH, Geering HP et al. Modeling of a three-way catalytic converter with respect to fast transients of λ-sensor relevant exhaust gas components. *Industrial & engineering chemistry research* 2004; 43(16): 4780–4788.
42. Germann HJ, Onder CH and Geering HP. Fast gas concentration measurements for model validation of catalytic converters. Technical Report (No. 950477), SAE Technical Paper, 1995.
43. Kumar P, Gu T, Grigoriadis K et al. Spatio-temporal dynamics of oxygen storage and release in a three-way catalytic converter. *Chemical Engineering Science* 2014; 111: 180–190.
44. Pontikakis G, Konstantas G and Stamatelos A. Three-way catalytic converter modeling as a modern engineering design tool. *Journal of Engineering for Gas Turbines and Power(Transactions of the ASME)* 2004; 126(4): 906–923.
45. Oh SH and Cavendish JC. Transients of monolithic catalytic converters. response to step changes in feedstream temperature as related to controlling automobile emissions. *Industrial & Engineering Chemistry Product Research and Development* 1982; 21(1): 29–37.
46. Chan S and Hoang D. Heat transfer and chemical reactions in exhaust system of a cold-start engine. *International journal of heat and mass transfer* 1999; 42(22): 4165–4183.
47. Schürholz K, Brückner D, Gresser M et al. Modeling of the three-way catalytic converter by recurrent neural networks. *IFAC-PapersOnLine* 2018; 51(15): 742–747.
48. Gonatas E and Stobart R. Prediction of gas concentrations in a three-way catalyst for on-board diagnostic applications. Technical Report No. 2005-01-0054, SAE Technical Paper, 2005.
49. Sanketi PR, Zavala JC, Hedrick J et al. A simplified catalytic converter model for automotive coldstart applications with adaptive parameter fitting. In *8th International Symposium on Advanced Vehicle Control, Taipei, Taiwan*.
50. Shaw II BT, Fischer GD and Hedrick JK. A simplified coldstart catalyst thermal model to reduce hydrocarbon emissions. *IFAC Proceedings Volumes* 2002; 35(1): 307–312.
51. Brandt EP, Wang Y and Grizzle JW. Dynamic modeling of a three-way catalyst for si engine exhaust emission control. *IEEE Transactions on control systems technology* 2000; 8(5): 767–776.
52. Balenovic M, Backx A and Hoebink J. On a model-based control of a three-way catalytic converter. Technical Report (No. 2001-01-0937), SAE Technical Paper, 2001.
53. Balenovic M, Backx T and De Bie T. Development of a model-based controller for a three-way catalytic converter. Technical Report (No. 2002-01-0475), SAE Technical Paper, 2002.
54. Shafai E, Roduner C and Geering HP. Indirect adaptive control of a three-way catalyst. Technical Report (No. 961038), SAE Technical Paper, 1996.
55. Pattas K, Stamatelos A, Pistikopoulos P et al. Transient modeling of 3-way catalytic converters. Technical Report (No. 940934), SAE Technical Paper, 1994.
56. Kiwitz P, Onder C and Guzzella L. Control-oriented modeling of a three-way catalytic converter with observation of the relative oxygen level profile. *Journal of Process Control* 2012; 22(6): 984–994.
57. Kumar P, Makki I, Kerns J et al. A low-dimensional model for describing the oxygen storage capacity and transient behavior of a three-way catalytic converter. *Chemical engineering science* 2012; 73: 373–387.
58. Auckenthaler TS, Onder CH and Geering HP. Online estimation of the oxygen storage level of a three-way catalyst.

Technical Report (No. 2004-01-0525), SAE Technical Paper, 2004.

59. Guzzella L and Onder C. *Introduction to modeling and control of internal combustion engine systems*. Springer Science & Business Media, 2009.
60. Frauhammer J, Klein H, Eigenberger G et al. Solving moving boundary problems with an adaptive moving grid method: Rotary heat exchangers with condensation and evaporation. *Chemical engineering science* 1998; 53(19): 3393–3411.
61. Ramanathan K and Sharma CS. Kinetic parameters estimation for three way catalyst modeling. *Industrial & Engineering Chemistry Research* 2011; 50(17): 9960–9979.